

Electronic Supplementary Material (ESI) for ChemComm

TiFeNb₁₀O₂₉₋₆ anode for high power and durable lithium-ion batteries

Guangshuo Wang, Yuanyuan Sun, Yonghua Sun, Chao Yan, Yuepeng Pang, Tao Yuan*, Shiyu Zheng*

School of Materials Science and Engineering, University of Shanghai for Science and Technology,

Shanghai 200093, China

* Corresponding authors.

E-mail addresses: T. Yuan (yuantao@usst.edu.cn); S. Zheng (syzheng@usst.edu.cn).

Experimental section

1. Material preparation

The TFNO powder was prepared by solid state reaction method. In brief, the stoichiometric TiO_2 (anatase, 99.9%), Fe_2O_3 (hematite, 99.8%), and Nb_2O_5 (AR, 99.9%), purchased from Aladdin Reagent Co. Ltd., were mixed and ground with a planetary ball milling apparatus, and then calcinated at 1000 °C for 10 h. As a control sample, pure $\text{Ti}_2\text{Nb}_{10}\text{O}_{29}$ (TNO) was prepared by the same way without adding Fe_2O_3 .

2. Materials characterization

Inductively coupled plasma optical emission spectroscopy (ICP-OES) (Agilent 5110) was used to obtain the exact composition of each chemical component in the TNO and TFNO samples. The structures and phases of the synthesized materials were measured by X-ray diffraction (XRD) with $\text{Cu K}\alpha$ radiation (BRUKER, D8 ADVANCE). Rietveld refinement of XRD was further performed by General Structure Analysis System (GSAS) to get the detailed structural information. The micro-morphology of the prepared samples was investigated by high-resolution transmission electron microscope HRTEM (JEM-2100F micro-scope) and corresponding energy dispersive spectroscopy (EDS). EPR spectra of the pristine TNO and TFNO samples were acquired using an EPR spectrometer (Bruker A320) at room temperature. The surface elements and corresponding valence states of the samples were analyzed using an XPS (Kratos Axis Ultra DLD).

3. Electrochemical measurements

The 2032-type coin cells were used to measure the electrochemical performance of

TFNO and TNO anodes. The electrode slurry was comprised of 85 wt % TFNO or TNO powder, 8 wt % carbon black, and 7 wt % polyvinylidene fluoride (PVDF) binder in N-methyl-2-pyrrolidone (NMP) (Sigma-Aldrich, 99.5%). Then, the slurry was spread on a Cu foil and dried in a vacuum oven at 80 °C overnight. The mass loading of the prepared electrode was controlled at $\sim 1.5 \text{ mg cm}^{-2}$.

The coin cells were assembled in a glovebox filled with Ar (O_2 and $\text{H}_2\text{O} < 0.1 \text{ ppm}$). The Li metal was used as the counter and reference electrodes, and the electrolyte consists of 1 M $\text{LiPF}_6/\text{EC}/\text{DMC}$ (1:1 in volume). The microporous polypropylene Celgard 3501 (Celgard, LLC Corp., USA) was used as a separator to separate the cathode (TFNO or TNO) and anode (Li metal) in the cell.

The electrochemical performance of TFNO and TNO were collected at room temperature (25 °C). The galvanostatic discharge-charge (GCD) was performed on a Neware CT-3008 eight-channel battery testing system. The voltage range (1-3 V vs. Li/Li^+) were adopted to test the electrochemical performance of the TFNO and TNO anodes. Here, the current rate of 1 C for both TFNO and TNO was equivalent to a current density of 200 mA g^{-1} . The current densities of charging and discharging are the same at a certain rate for the rate testing. The galvanostatic intermittent titration technique (GITT) was also performed on the Neware CT-3008 eight-channel battery testing system at a pulse current of 10 mA g^{-1} for 30 min between 2 h of relaxation. The electrochemical impedance spectroscopy (EIS) and cyclic voltammetry (CV) were conducted using a Gamry Reference 6000 (Gamry Co., U.S.A.) electrochemical station. The applied frequency for EIS is from 100 kHz to 100 mHz.

4. Computational method

Density functional theory (DFT) with the Vienna ab initio simulation package (VASP).^{1, 2} The projector-augmented-wave (PAW) potentials were used while the generalized gradient approximations (GGA) of Perdew-Burke-Ernzerhof (PBE) were applied for the exchange-correlation functional. The cutoff energy was set to 500 eV, and the gamma point was applied in our calculations. The force on each atom less than 0.01 eV/Å was set for convergence criterion of geometry relaxation. The Climbing Image-Nudged Elastic Band (CI-NEB) methods were employed to calculate the migration barriers.

Table S1

Table S1 ICP-OES results of the pristine TNO and TFNO samples

Theoretical Chemical	Measured atomic ratio		
Formula	Ti	Fe	Nb
$\text{Ti}_2\text{Nb}_{10}\text{O}_{29}$	1.989	0	10.013
$\text{TiFeNb}_{10}\text{O}_{29-6}$	0.994	1.015	10.008

Table S2

Table S2 Crystallographic parameters and other phase information of the TNO and TFNO samples refined by Rietveld method.

	a/Å	b/Å	c/Å	V/Å ³	other phases	molar ratio	Rp%	wRp%
Ti ₂ Nb ₁₀ O ₂₉	15.5826	3.8219	20.5961	1127.4645	none		5.61	7.28
TiFeNb ₁₀ O ₂₉	15.5762	3.8242	20.5979	1128.8121	Ti ₂ Nb ₁₀ O ₂₉ orthorhombic	11%	2.47	3.12
					FeNbO ₄	5%		

Figure S1

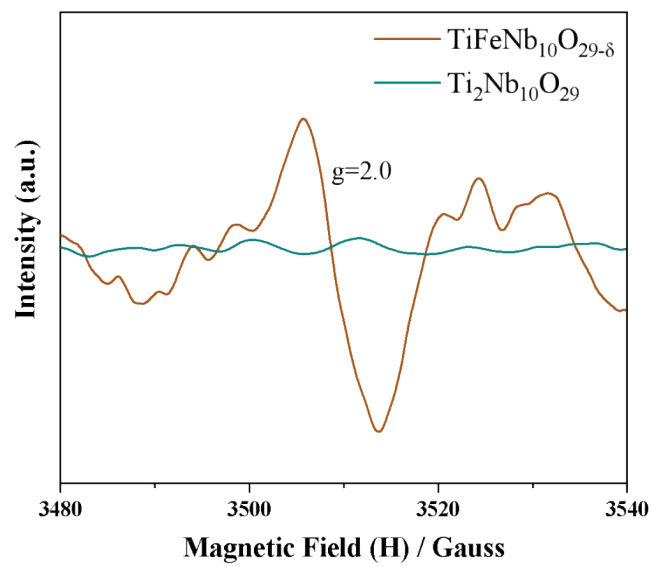


Figure S1 EPR spectra of the pristine TNO and TFNO samples.

Figure S2

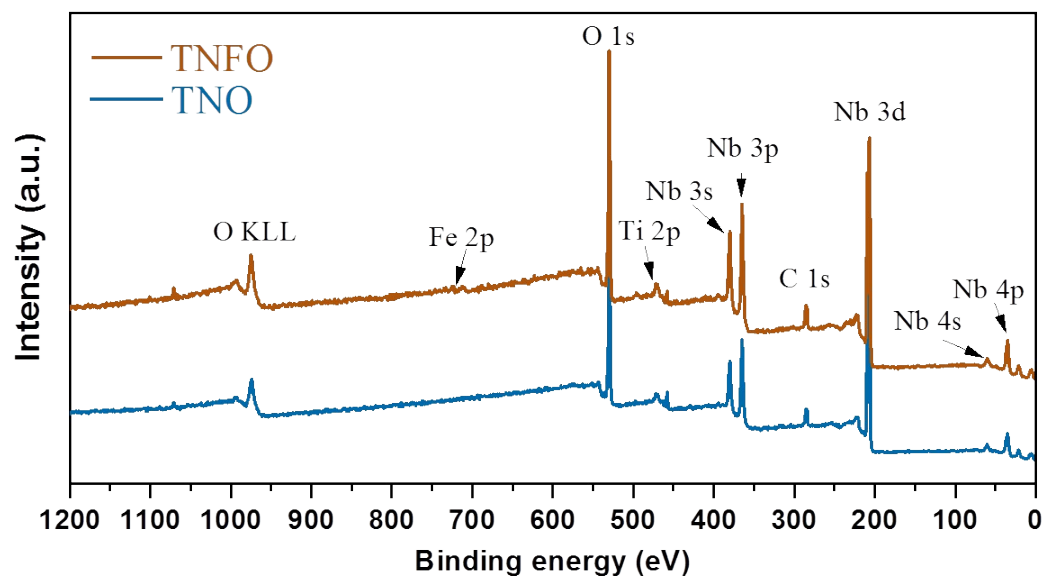


Figure S2 XPS spectra of TNO and TFNO samples.

Table S3

Table S3 Nb 3d composition from high-resolution XPS spectra

		Nb ⁵⁺ 3d _{3/2}	Nb ⁴⁺ 3d _{3/2}	Nb ⁵⁺ 3d _{5/2}	Nb ⁴⁺ 3d _{5/2}
Binding Energy (eV)		209.7	208.7	206.9	206.2
ratios (% at.)	TNO	37.3	--	62.7	--
	TFNO	29.0	10.3	40.6	20.1

Table S4

Table S4 Ti 2p composition from high-resolution XPS spectra

		Ti ⁴⁺ 2p _{1/2}	Ti ³⁺ 2p _{1/2}	Ti ⁴⁺ 2p _{3/2}	Ti ³⁺ 2p _{3/2}
Binding Energy (eV)		464.4	463.4	458.7	458.1
ratios (% at.)	TNO	30.4	--	69.9	--
	TFNO	18.7	5.5	68.4	7.4

Figure S3

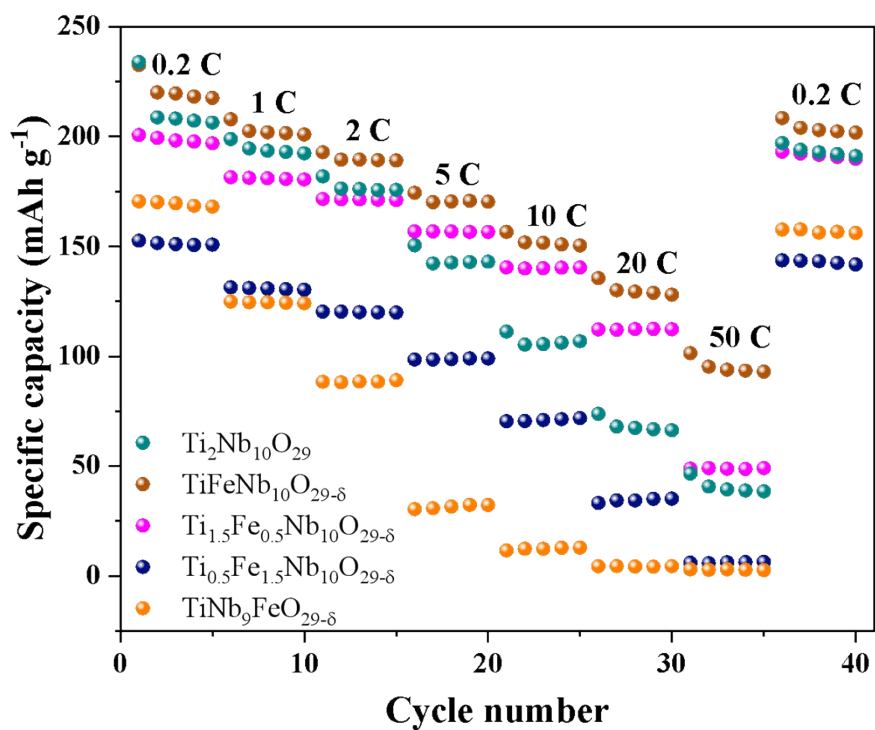


Figure S3 Rate-cycle capabilities of $\text{Ti}_2\text{Nb}_{10}\text{O}_{29}$, $\text{TiFeNb}_{10}\text{O}_{29-\delta}$, $\text{Ti}_{1.5}\text{Fe}_{0.5}\text{Nb}_{10}\text{O}_{29-\delta}$, $\text{Ti}_{0.5}\text{Fe}_{1.5}\text{Nb}_{10}\text{O}_{29-\delta}$, and $\text{TiNb}_9\text{FeO}_{29-\delta}$ electrodes.

Table S5

Table S5 The comparison of electrochemical behaviors of titanium niobium oxide anodes

Materials	Low rate capacity (mAh g⁻¹)	High rate capacity (mAh g⁻¹)	Cycle retention	Ref.
TiFeNb ₁₀ O _{29-δ}	225 (0.2C)	100 (50C)	86.7% (10C 1000cycles)	This work
Ti ₂ Nb ₁₀ O ₂₉ microrods	205 (0.5C)	80 (20C)	66% (10C 500cycles)	3
Ti ₂ Nb ₁₀ O ₂₉ nanoparticles	200 (0.5C)	100 (10C)	66.7% (1C 200cycles)	4
TiNb ₂₄ O ₆₂ /NC nanowires	218 (0.5C)	177 (6C)	92.2% (10C 900cycles)	5
macroporous TiNb ₂ O ₇	206 (1C)	84 (20C)	82% (10C 1000cycles)	6
TiNb ₆ O ₁₇ nanospheres	214.4 (0.5C)	127.3 (5C)	75.2% (0.5C 150cycles)	7

Figure S4

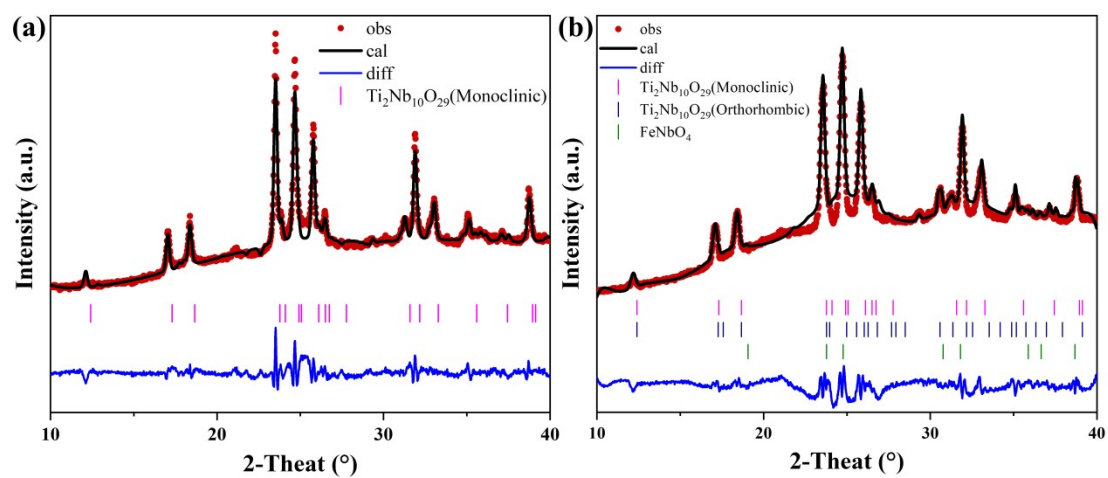


Figure S4 Rietveld refinement patterns of the XRD data for (a) TNO and (b) TFNO electrodes at the full lithiation state (discharge to 1 V).

Table S6

Table S6 Crystallographic parameters of the TNO and TFNO electrodes at the full lithiation state (discharge to 1 V) refined by Rietveld method.

	a/Å	b/Å	c/Å	V/Å ³	ΔV/%
Ti ₂ Nb ₁₀ O ₂₉	15.5542	3.8412	20.6260	1133.4460	0.5305
TiFeNb ₁₀ O ₂₉	15.5398	3.8416	20.6278	1133.2872	0.3946

Figure S5

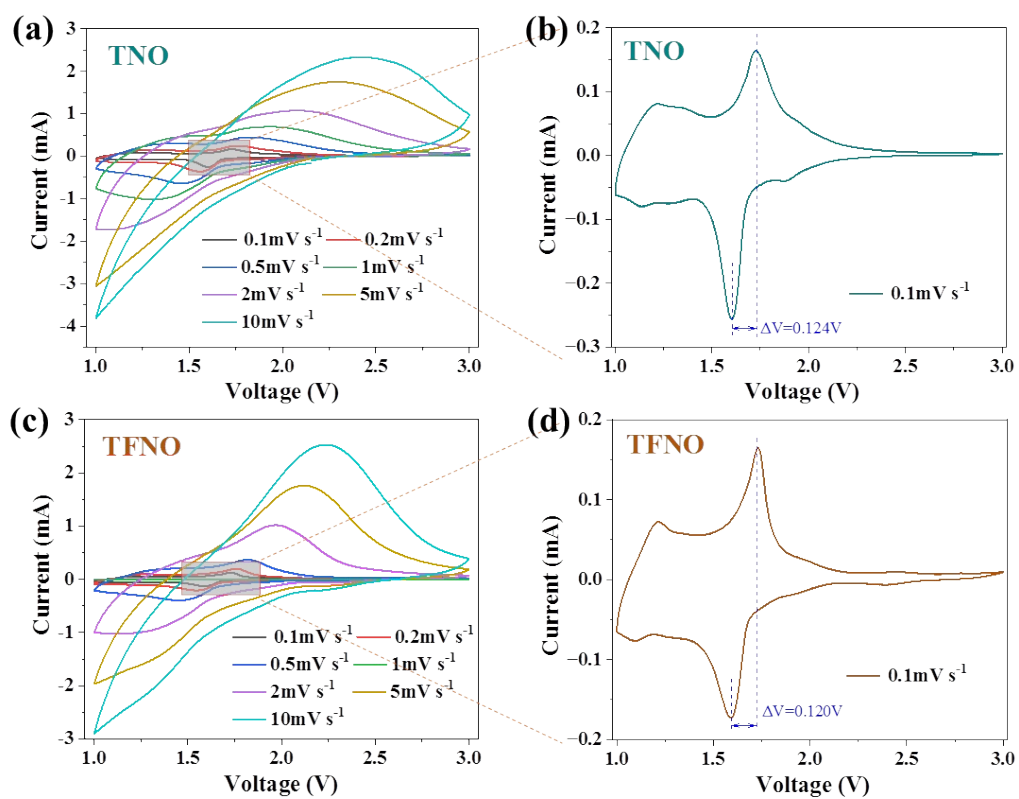


Figure S5 CV curves of the (a) TNO and (c) TFNO electrodes at various scan rates from 0.1 mV s⁻¹ to 10 mV s⁻¹; and the magnified CV curves with scan rate of 0.1 mV s⁻¹ for (b) TNO and (d) TFNO electrodes.

Table S7

Table S7 Resistance values of TNO and TFNO electrodes based on the EIS fitting results

	R1 (Ω)	R2+R3 (Ω)
TNO	2.753	23.102
TFNO	2.599	9.206

R1: ohmic resistance;

R2+R3: polarization and charge-transfer resistances.

Figure S6

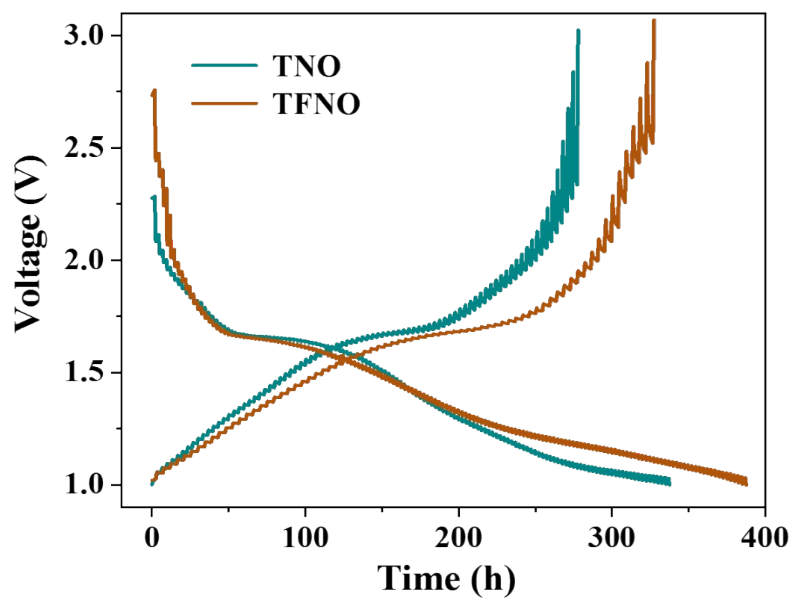


Figure S6 GITT curves for the TNO and TFNO electrodes.

References

1. A. S. Botana and M. R. Norman, *Phys. Rev. Mater.*, 2019, **3**, 044001.
2. L. Chaput, P. Pécheur and H. Scherrer, *Phys. Rev. B*, 2007, **75**, 045116.
3. X. Xia, S. Deng, S. Feng, J. Wu and J. Tu, *J. Mater. Chem. A*, 2017, **5**, 21134-21139.
4. C. D. Gu, X. H. Xia, J. P. Tu, X. L. Wang and L. Zhang, *Sustainable Mater. Technol.*, 2021, **28**, e00272.
5. H. Yu, X. Cheng, H. Zhu, R. Zheng, T. Liu, J. Zhang, S. Miao, X. Ying and S. Jie, *Nano Energy*, 2018, **54**, 227-237.
6. X. Cheng, Y. Zhao, A. Lushington, J. Gao, Q. Li, P. Zuo, B. Wang, Y. Gao and Y. Ma, *Nano Energy*, 2017, **34**, 15-25.
7. Y. Yuan, H. Yu, X. Cheng, R. Zheng, T. Liu, N. Peng, N. Long, M. Shui and J. Shu, *Chem. Eng. J.*, 2019, **374**, 937-946.